

A Novel Paradigm for Neural Computation: X-Net with Learnable Neurons and Adaptable Structure

Yanjie Li^{1,2}, Weijun Li^{1,2,3*†}, Lina Yu^{1†}, Min Wu¹, Jinyi Liu^{1,2},
Wenqiang Li^{1,2}, Meilan Hao¹

^{1*}ANMLAB, Institute of Semiconductors, Chinese Academy of Sciences,
Haidian, Beijing, 100083, Beijing, China.

²School of Electronic, Electrical and Communication Engineering,
University of Chinese Academy of Sciences, Huairou, Beijing, 101408,
Beijing, China.

³School of Integrated Circuits, University of Chinese Academy of
Sciences, Huairou, Beijing, 101408, Beijing, China.

*Corresponding author(s). E-mail(s): wjli@semi.ac.cn;

Contributing authors: liyanjie@semi.ac.cn; yulina@semi.ac.cn;
wumin@semi.ac.cn; liujingyi@semi.ac.cn; liwenqiang@semi.ac.cn;
mlh@semi.ac.cn;

†These authors contributed equally to this work.

Abstract

Artificial neural networks (ANNs) have permeated various disciplinary domains, ranging from bioinformatics to financial analytics, where their application has become an indispensable facet of contemporary scientific research endeavors. However, the inherent limitations of traditional neural networks arise due to their relatively fixed network structures and activation functions. 1, The type of activation function is single and relatively fixed, which leads to poor "unit representation ability" of the network, and it is often used to solve simple problems with very complex networks; 2, the network structure is not adaptive, it is easy to cause network structure redundant or insufficient. To address the aforementioned issues, this study proposes a novel neural network called X-Net. By utilizing our designed Alternating Backpropagation mechanism, X-Net dynamically selects appropriate activation functions based on derivative information during training to enhance the network's representation capability for specific tasks. Simultaneously, it accurately adjusts the network structure at the neuron level to accommodate tasks of varying complexities and reduce computational costs. Through a series

of experiments, we demonstrate the dual advantages of X-Net in terms of reducing model size and improving representation power. Specifically, in terms of the number of parameters, X-Net is only 3% of baselines on average, and only 1.4% under some tasks. In terms of representation ability, X-Net can achieve an average $R^2=0.985$ on the fitting task by only optimizing the activation function without introducing any parameters. Finally, we also tested the ability of X-Net to help scientific discovery on data from multiple disciplines such as society, energy, environment, and aerospace, and achieved concise and good results.

Keywords: Neural Networks, Activation function learning, Dynamic adjustment of structure

1 Introduction

In the field of artificial intelligence, scientists have been studying artificial neural networks almost as old as AI itself. Since the 1940s, the development of neural networks has had ups and downs. Since Warren McCulloch and Walter Pitts proposed the MP model, Frank Rosenblatt, Marvin Minsky Seymour Papert, Hinton, David Rumelhart, Sepp Hochreiter, Xavier Glorot, Yoshua Bengio, and a series of scientists in the process of the development of the neural network has played a very important role. All of them proposed or solved a series of important problems in the development of artificial neural networks. In today's mainstream artificial neural network paradigm, once the structure is initialized, its activation function and network structure are fixed during the training process. This makes it difficult for the neural network to accurately adapt to the task. As a result, the network structure is either redundant or insufficient. Especially in the current context of various large models emerging endlessly and people blindly increasing the scale of neural networks in pursuit of more powerful performance. **It is necessary to study a new neural network with dynamic learnable activation functions and adaptive adjustment of network structure.** This is also a problem that future artificial intelligence research must face. Because human computing power is ultimately limited, the scale of the model cannot be expanded indefinitely.

Some traditional network structure optimization algorithms treat the network structure as the hyperparameters of neural networks and then use some optimization algorithms to optimize these hyperparameters. Such as evolutionary algorithms[1] and Bayesian optimization algorithms[2]. Recently, some automatic design methods of network structure have been proposed which are more flexible than the traditional hyperparameter optimization methods. Zoph and Le [3] define recurrent neural networks (RNNS) that generate a neural network architecture for a specific target problem, optimize the RNNS by using a strategy gradient approach, and find a good neural network architecture. The work of Real et al. 2017[4]; Suganuma, [5] uses evolutionary algorithms to optimize layer-to-layer neuronal connections to build high-performance neural network architectures. [6] consider a probability distribution that generates

network structures, and optimizes the parameters of the distribution instead of directly optimizing the network structure. The Jagtap[7] paper presents a new type of neural network, Kronecker Neural Networks (Kronecker NNs), which forms a general framework for neural networks with adaptive activation functions. In addition, the paper proposes a Rowdy activation function, which aims to eliminate any saturated regions by injecting sinusoidal fluctuations, which include trainable parameters. Agostinelli[8] designed a new form of parametric piecewise linear activation functions that are learned independently for each neuron using gradient descent and can represent both convex and non-convex functions of the input.

We propose a new neural network called X-Net. Both the activation function and the network structure of X-Net are dynamically adaptive. While learning the type of activation function, the network structure can also be adjusted accurately at the neuron level. So that the neural network structure can automatically grow or shrink according to the demand to adapt to different difficult tasks. We design X-Net mainly from the following two aspects:

- Increase the type of activation function to improve the unit representation ability of the network.
- The network structure is dynamically adjusted in real-time, which makes the network structure match the task requirements accurately and reduces the occurrence of parameter redundancy and insufficiency.

First, we propose a new model that allows X-Net to theoretically use any differentiable function as the activation function, and the type of activation function can be selected in real-time according to the needs of the task under the guidance of the gradient during the network training. In particular, in the process of selecting the activation function, the precise adjustment of the network structure can be realized, so that the network structure and scale can be adapted to the current task as much as possible.

In summary, the X-Net model not only opens up a new research approach in the field of neural networks but also sets up a new technical standard for building truly adaptive intelligent systems. It is expected that X-Net can play its value in various fields in the future and promote the progress and development of mankind. In the end, we hope that our research will throw a brick to attract jade and stimulate enthusiasm for this new type of neural network.

2 Results

Evaluating X-Net. In order to comprehensively evaluate the performance of X-Net, we make a comprehensive evaluation of X-Net in terms of fitting ability and classification ability. In particular, we also test X-Net’s ability to scientific discovery on datasets from various disciplines such as environment and energy.

2.1 Fit ability evaluation

We compare X-Net with support vector regression(SVR), ANN, Kronecker NN, and Shinichi[6] four excellent regression algorithms.

Table 1
COMPARISON OF EXTRAPOLATION BETWEEN X-NET, ANN, AND SVR.

Benchmark	X-Net		ANN		SVR		Kronecker NN		Shinichi[6]		X-Net (No parameters)	
	In [-2,2]	Not in [-2,2]	In [-2,2]	Not in [-2,2]	In [-2,2]	Not in [-2,2]	In[-2,2]	Not in [-2,2]	In [-2,2]	Not in [-2,2]	In [-2,2]	Not in [-2,2]
Nguyen-1	1.00 \pm 0.0	1.00 \pm 0.0	0.99 \pm 0.08	-29.34 \pm 4.23	0.99 \pm 0.02	-59.33 \pm 1.21	0.99 \pm 0.05	-32.45 \pm 1.92	0.99 \pm 0.02	-19.29 \pm 0.84	1.00 \pm 0.00	1.00 \pm 0.00
Nguyen-2	1.00 \pm 0.00	1.00 \pm 0.00	0.99 \pm 0.04	-111.57 \pm 14.34	0.99 \pm 0.05	-441.08 \pm 3.53	0.99 \pm 0.03	-167.28 \pm 4.31	0.99 \pm 0.03	-147.26 \pm 2.01	1.00 \pm 0.00	1.00 \pm 0.00
Nguyen-3	0.99 \pm 0.06	0.96 \pm 0.04	0.99 \pm 0.05	-553.86 \pm 79.18	0.99 \pm 0.07	-397 \pm 04.22	0.99 \pm 0.02	-504.81 \pm 8.54	0.99 \pm 0.01	-382.64 \pm 6.30	0.99 \pm 0.02	0.94 \pm 0.03
Nguyen-4	0.99 \pm 0.09	0.94 \pm 0.06	0.98 \pm 0.10	-2452.16 \pm 282.23	0.99 \pm 0.08	-5107 \pm 32	0.99 \pm 0.03	-3048.24 \pm 302	0.99 \pm 0.02	-3012.62 \pm 26.44	0.99 \pm 0.03	0.84 \pm 0.09
Nguyen-5	0.99 \pm 0.04	-0.12 \pm 0.08	0.99 \pm 0.08	-9.76 \pm 0.82	0.57 \pm 0.07	-19.81 \pm 0.13	0.99 \pm 0.07	-16.73 \pm 0.93	0.99 \pm 0.04	-14.28 \pm 0.94	0.86 \pm 0.07	0.10 \pm 0.08
Nguyen-6	1.00 \pm 0.00	1.00 \pm 0.00	0.99 \pm 0.07	-8.49 \pm 1.30	0.99 \pm 0.05	-2.34 \pm 0.08	0.99 \pm 0.02	-12.86 \pm 0.79	0.99 \pm 0.04	-13.72 \pm 0.74	1.00 \pm 0.00	1.00 \pm 0.00
Nguyen-7	0.99 \pm 0.02	0.94 \pm 0.03	0.99 \pm 0.06	0.62 \pm 0.09	0.99 \pm 0.03	-53.00 \pm 0.46	0.99 \pm 0.03	-0.29 \pm 0.02	0.99 \pm 0.06	0.12 \pm 0.03	0.99 \pm 0.03	0.62 \pm 0.08
Nguyen-8	1.00 \pm 0.00	1.00 \pm 0.00	0.99 \pm 0.01	0.71 \pm 0.02	0.96 \pm 0.05	-47.52 \pm 0.20	0.99 \pm 0.03	0.16 \pm 0.01	0.99 \pm 0.03	0.31 \pm 0.01	1.00 \pm 0.00	1.00 \pm 0.00
Nguyen-9	1.00 \pm 0.00	1.00 \pm 0.00	0.99 \pm 0.05	-3.31 \pm 0.49	0.98 \pm 0.04	-48.52 \pm 0.19	0.99 \pm 0.06	-10.17 \pm 0.89	0.99 \pm 0.04	-11.27 \pm 1.20	1.00 \pm 0.00	1.00 \pm 0.00
Nguyen-10	1.00 \pm 0.00	1.00 \pm 0.00	0.99 \pm 0.09	-15.56 \pm 1.22	0.98 \pm 0.41	-3.05 \pm 0.41	0.99 \pm 0.05	-28.75 \pm 0.99	0.99 \pm 0.02	-16.88 \pm 0.96	1.00 \pm 0.00	1.00 \pm 0.00
Nguyen-11	1.00 \pm 0.00	1.00 \pm 0.00	0.99 \pm 0.02	-124985 \pm 4476.20	0.99 \pm 0.02	-858911 \pm 10006	0.99 \pm 0.1	-204823 \pm 3013	0.99 \pm 0.08	-116424 \pm 822	1.00 \pm 0.00	1.00 \pm 0.00
Nguyen-12	0.99 \pm 0.09	-2.34 \pm 0.10	0.99 \pm 0.20	-599.34 \pm 28.44	0.99 \pm 0.20	-8466 \pm 244.55	0.99 \pm 0.07	-1027.13 \pm 20.66	0.99 \pm 0.08	-646.22 \pm 12.64	0.99 \pm 0.09	0.16 \pm 0.04
Average	0.996	0.531	0.989	-10730.58	0.950	-72795	0.990	-17472	0.990	-10057	0.985	0.805

- **Support Vector Regression (SVR)**. SVR is characterized by the use of the kernel, sparse solution, and VC to control the margin and the number of support vectors. One of the main advantages of SVR is that its computational complexity does not depend on the dimensions of the input space. In addition, it has excellent generalization ability and high prediction accuracy.
- **Artificial Neural Network (ANN)**. ANN is a kind of neural network which uses a backpropagation algorithm to update parameters. This network is one of the most widely used neural networks and is the foundation of deep learning. ANN has achieved excellent results in the field of regression.
- **Kronecker NN**. Kronecker NN is a new neural network framework using Kronecker products for efficient wide networks with fewer parameters. Kronecker NN also introduces the Rowdy activation function, adding trainable sinusoidal fluctuations for better data fitting.
- **Shinichi[6]**. This method generates the probability distribution of the network structure and then optimizes the parameters of the distribution, rather than optimizing the network structure directly.

2.1.1 Analysis of fitting ability

We tested the above four algorithms on the Nguyen data set. The dataset contains 12 curves, each of which is a mathematical formula. See the appendix for details. We used R^2 to test the fitting ability of our algorithm and SVR, ANN, Kronecker NN, and Shinichi[6]. The formula for R^2 is as follows(1).

$$R^2 = 1 - \frac{\sum_{i=0}^N (y_i - \hat{y}_i)^2}{\sum_{i=0}^N (y_i - \bar{y})^2}. \quad (1)$$

where y_i is the true label value of the i^{th} sampling point, \hat{y}_i is the value predicted by the model for the i^{th} data, \bar{y} is the mean of the true values y . The closer R^2 is to 1

the better the algorithm fits the target curve, and conversely, the farther R^2 is from 1, the worse the algorithm fits the target curve. The specific results are shown in Table 1[-2,2]. From the table, we can clearly find that our algorithm has better inherited the powerful nonlinear fitting ability of the neural network, and its fitting ability is not weaker than that of excellent regression algorithms such as SVR, ANN, Kronecker NN and Shinichi[6].

Table 2

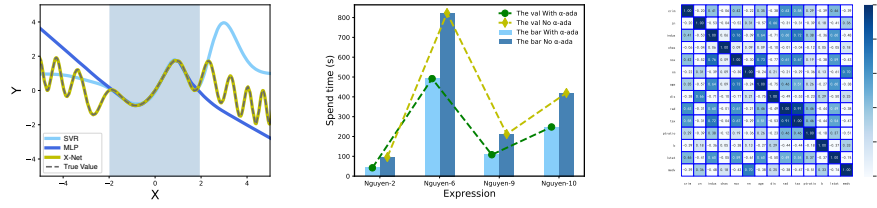
A COMPARATIVE ANALYSIS IS PRESENTED, FOCUSING ON THE ACCURACY AND COMPLEXITY OF THE FINAL NETWORK STRUCTURES ACROSS FOUR ALGORITHMS IN BOTH REGRESSION AND CLASSIFICATION TASKS.

REGRESSION												
Benchmark	X-Net			ANN			Kronecker NN			Shinichi[6]		
	Acc	Nod	Para	Acc	Nod	Para	Acc	Nod	Para	Acc	Nod	Para
Nguyen-1	1.0	5	22	0.99	14	78	0.99	12	61	0.99	12	52
Nguyen-2	1.0	9	38	0.99	18	118	0.99	16	97	0.99	15	79
Nguyen-3	1.0	14	58	0.99	18	118	0.99	14	78	0.99	11	47
Nguyen-4	0.99	20	82	0.98	28	253	0.99	24	193	0.99	18	115
Nguyen-5	0.99	5	16	0.99	26	222	0.99	28	253	0.99	30	289
Nguyen-6	0.99	5	18	0.99	8	33	0.99	8	33	0.99	7	27
Nguyen-7	1.0	5	16	0.99	12	61	0.99	10	46	0.99	8	37
Nguyen-8	0.99	1	4	0.99	16	97	0.99	16	97	0.99	12	61
Nguyen-9	0.99	3	10	0.99	40	481	0.99	28	253	0.99	21	139
Nguyen-10	0.99	4	14	0.99	130	4468	0.99	80	1761	0.99	56	919
Nguyen-11	0.99	1	6	0.99	16	97	0.99	20	141	0.99	12	65
Nguyen-12	1.0	9	40	0.99	16	97	0.99	12	61	0.99	14	73
Average	0.996	6.75	27	0.989	28.50	510.25	0.990	21.5	256.17	0.990	18	158.58
CLASSION												
Iris	0.987	26	28	0.980	51	828	0.983	38	632	0.986	32	546
Mnist(6-dim)	0.894	55	166	0.886	201	11713	0.888	142	6735	0.889	128	6022
Mnist	0.995	316	4728	0.992	488	158260	0.992	463	117119	0.990	444	100626

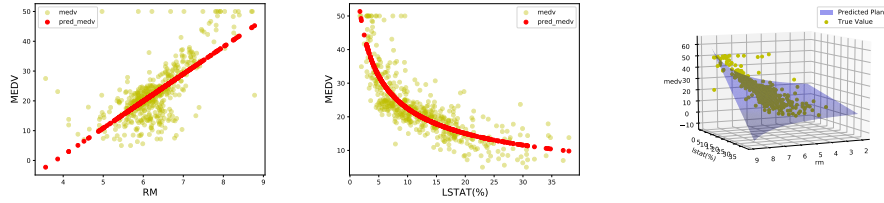
2.1.2 Analysis of extrapolation ability

It is not enough to fit the given data well in the regression analysis. We also need the model to have good extrapolation ability. For example, we only have the data of x in the range $[-2, 2]$ and the corresponding value of y . We use this data as a training set to train the model. We need a model that not only works well in the range $[-2, 2]$, but also fits well outside the range $[-2, 2]$ (e.g., $[-5, 5]$). We call this ability of the model extrapolation ability.

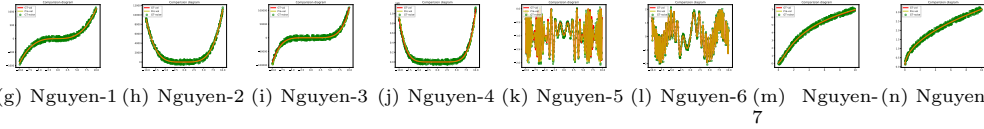
To test the extrapolation ability of the model, we sampled x in the range of $[-2, 2]$ and obtained the corresponding y values. These data are then used to train each of the three algorithms X-Net, SVR, ANN, Kronecker NN, and Shinichi[6]. Finally, we



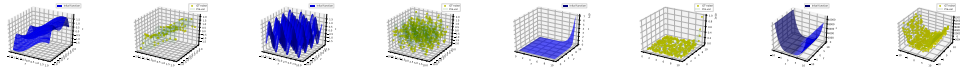
(a) Fitting capability and extrapolation (b) Performance of the Ada- α Activation Function (c) Boston Housing Price Data Correlation Matrix.



(d) Predicting housing prices using the 'RM' (e) Predicting housing prices using the 'LSTAT' (f) Predicting housing prices using 'RM' and 'LSTAT'



(g) Nguyen-1 (h) Nguyen-2 (i) Nguyen-3 (j) Nguyen-4 (k) Nguyen-5 (l) Nguyen-6 (m) Nguyen-7 (n) Nguyen-8



(o) Nguyen-9-TV (p) Nguyen-9-PRE (q) Nguyen-10-TV (r) Nguyen-10-PRE (s) Nguyen-11-TV (t) Nguyen-11-PRE (u) Nguyen-12-TV (v) Nguyen-12-PRE

Figure 1: Figure a illustrates the fitting capabilities and extrapolation properties on Eq. Nguyen-6 $\sin(x^2 + x) + \sin(x)$ of various algorithms; Figure b depicts the change in algorithmic efficiency before and after the use of ada- α ; Figure c presents the correlation matrix among different variables in the Boston housing price prediction; Figure d demonstrates the schematic representation of housing price predictions using the variable 'RM'. From the figure, it can be deduced that the housing prices are directly proportional to the variable 'RM', which is consistent with the findings presented in Figure c; Figure e displays the illustrative results of predicting housing prices using the variable 'LSTAT'. Figure f showcases the schematic representation of predicting housing prices using both 'RM' and 'LSTAT'. Figures g through n exhibit the prediction results of X-Net on univariate expressions; Figures o through v display the prediction outcomes of X-Net on multivariate expressions, where '-TV' denotes true values and '-PRE' represents predicted values.

sampled x on $[-5, 5]$ as a test set to test the three models and recorded the goodness-of-fit of the three algorithms in the interval $[-2, 2]$ and outside the interval respectively, and the specific results are shown in Table 1. From the table, we can find that our algorithm is superior to SVR, ANN, Kronecker NN, and Shinichi[6] in extrapolation ability. The main reason for this is that the activation function of X-Net is more diverse and has more powerful representation ability. And the purpose of our algorithm is not only fitting but to find a mathematical expression that can well represent these data. And, the expression has good extrapolation, and its representation ability will not be significantly affected by the change in the x value range. The simple diagram is shown in Fig. 1a

2.1.3 Diversity activation function representation capability analysis

To explore the powerful representation power of activation function diversity, we designed a unique test scheme: remove the weight parameter W and bias term B from a neural network, and try to fit the data in Table 1 purely by selecting and optimizing the activation function type of each neuron node, taking advantage of the nonlinear nature of these activation functions. This process only depends on the nonlinear expressive power of the activation function. From the last column of Table 1 ‘X-Net (No parameters)’, we can find that X-Net can make a good fit to the data and show good extrapolation even when no parameters are introduced. This experiment strongly demonstrates the powerful nonlinear representation ability of our neural network.

2.1.4 Comparison of network structure complexity

Artificial neural networks have a fixed network structure and a number of nodes, which can easily lead to redundancy in parameters and nodes, greatly slowing down the convergence efficiency of the neural network. In contrast, X-Net is more flexible, with a dynamically changing network structure and the number of nodes that can be adaptively adjusted based on the complexity of the problem. This greatly alleviates the problem of redundancy in nodes and parameters in ordinary neural networks. In order to test the complexity of the model obtained by four algorithms X-Net, ANN, Kronecker NN, and Shinichi[6] on the same task, we stop the training when $R^2 = 0.99$, and count the number of nodes and parameters used by the four networks at this time. The specific statistical results are shown in Table 2. From Table 2, it is evident that in fitting the Nguyen data set, the ANN necessitates approximately fourfold the node count in comparison to X-Net and demands almost a twentyfold increase in the quantity of parameters for optimization. The Kronecker NN algorithm demands roughly thrice the node count relative to X-Net and entails nearly a decuple increase in the number of parameters relative to X-Net. Shinichi[6] requires about three times as many nodes and five times as many parameters as X-Net.

2.2 Classification ability evaluation

The classification task stands as a quintessential sub-domain within the realm of machine learning. Consequently, gauging the classification performance of algorithms

becomes imperative. To validate the classification efficacy of X-Net, we employed the Iris dataset and the MNIST handwritten digit recognition dataset as our experimental datasets. We juxtaposed the performance of X-Net with the ANN. On the MNIST dataset, we conducted two distinct experiments: initially, we employed PCA to dimensionally reduce the data, transmuting the images from a 28x28 dimension down to 6 dimensions, and subsequently classified using the reduced data. The secondary experiment involved direct classification without any dimension reduction. Table 2 meticulously delineates the performance comparison between X-Net and Others on both the Iris and MNIST datasets. The outcomes suggest that X-Net marginally outperforms the conventional ANN across all three classification tasks. Regarding network structural complexity, X-Net surpasses its counterpart. Taking the Iris dataset as a case in point, the neuron count of X-Net is merely half that of ANN, with its parameter magnitude being a mere tenth of that of ANN. On the MNIST dataset, In the experimentation employing PCA, the node count of X-Net is but a quarter of ANN, and its parameter magnitude stands at a mere 1.4% (1/70) of ANN. In experiments without dimension reduction, the node count of X-Net amounts to two-thirds that of ANN, while the parameter count is a mere 2.9% (3/100) of ANN. In summation, X-Net not only excels in classification tasks but also showcases a substantially reduced network structural complexity compared to the traditional ANN. Similarly, compared to Kronecker NN and Shinichi[6], X-Net also has significant advantages.

2.3 Used in scientific discovery

2.3.1 Modeling in economics (Boston house price forecast[9])

The Boston house price forecast data set is a very classic data set in the field of machine learning. Although it is simple, it can test the comprehensive performance of the algorithm well. Each sample in the Boston housing price data set is composed of 12 characteristic variables such as 'CRIM', 'ZN', and housing price MEDV. The thermal map of the correlation coefficient between each variable is shown in the figure 1c. From the heat map 1c, we can find that the variable 'RM' (the number of rooms per house) has the highest correlation coefficient with the MEDV(housing price), which is 0.70, showing a positive correlation with the housing price. In contrast, the variable 'LSTAT' (how many people in the area are classified as low-income) has a minimum correlation coefficient of -0.74 with housing prices, showing a negative correlation with housing prices.

We use RM to forecast the house price MEDV, and the final formula was as follows(2):

$$MEDV = 9.10RM - 34.67(RM \geq 2) \quad (2)$$

The predicted results are shown in Fig. 1d. From Formula 2, we can find that the final expression obtained by our algorithm can well reflect the positive correlation between RM and housing price.

We used LSTAT as input to predict housing prices using X-Net and finally got formula (3), from which we could see that the formula also well reflected the negative

correlation between LSTAT and MEDV. Show in Fig 1e.

$$MEDV = \frac{81.39}{(LSTAT + 0.44)^{0.44}} - 6.54(0 \leq LSTAT \leq 100) \quad (3)$$

Finally, we use RM and LSTAT as inputs to predict housing prices, and we get formula (4), And the predicted results are shown in Fig. 1f

$$MEDV = \frac{15.6(0.48RM - 13.21)}{2.36LSTAT - 24.53} + 9.97 \quad (4)$$

From Formula 4, we can clearly find that the housing price is directly proportional to the variable RM and inversely proportional to the variable LSTAT. That is the more rooms in the house, the more expensive the house, the more low-income people in the community, and the lower the price. The result of this prediction is completely in line with the facts. The above results prove that our algorithm can well reflect the relationship between each variable and the result even for multiple variables.

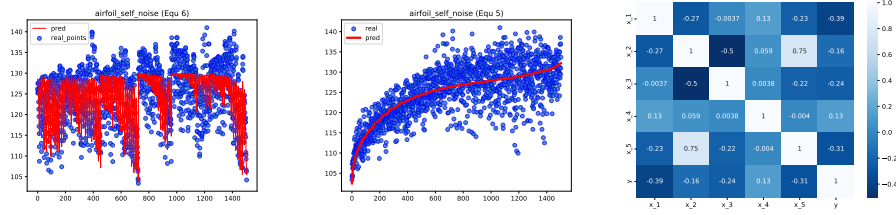
2.3.2 Modeling in space science (Airfoil-self-noise)[10]

We use the airfoil-self-noise data set to conduct practical tests on the algorithms for our paper. The airfoil-self-noise data set consists of six dimensions, of which five dimensions are feature data, namely Frequency (x_1), Angle of attack (x_2), Chord length (x_3), Free-stream velocity (x_4), and Suction side displacement thickness (x_5). Our goal is to predict the Scaled sound pressure level (Y) data through the above five features. The formula discovered by applying our algorithm is shown in the following text, and the two equations we found are presented below (rounded to two decimal places):

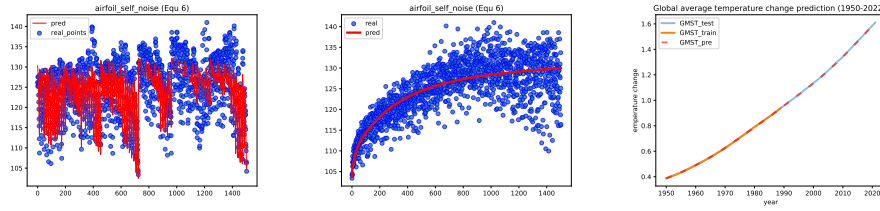
$$Y = 97.7 + \frac{-x_2 + x_4 + 292}{x_1 * x_3 * x_5 + 10.5} \quad (5)$$

$$Y = 130 - \frac{167.37}{\frac{x_4}{x_1 * x_3 * x_5} + 5.67} \quad (6)$$

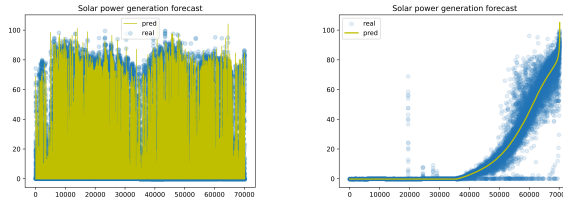
The comparison between the predicted data and the real data for the two formulas above is shown in Figure 2. Figure 2a and Figure 2b demonstrate the fitting results of Equation 5. Note: To more clearly present the fitting outcomes of Equation 5, without altering the R^2 value, we sorted the data points in Figure a based on the predicted values y_{pre} in ascending order, resulting in Figure 2b. From Figure 2b, it is evident that Equation 5 passes through the center of the data points, robustly fitting the data points. Figure 2d and Figure 2e depict the fitting results of Equation 6, with Figure 2e undergoing the same data processing as Figure 2b. From equation 5 above, we can observe that the predicted value y is directly proportional to x_1 , x_2 , x_3 , and x_5 , and inversely proportional to x_4 . The situation reflected in the formula is consistent with the correlation coefficient heatmap 2c. From the graph, we can clearly see that only the fourth feature variable is directly proportional to the predicted result Y , while the other variables are inversely proportional to the result Y . Especially in equation 6,



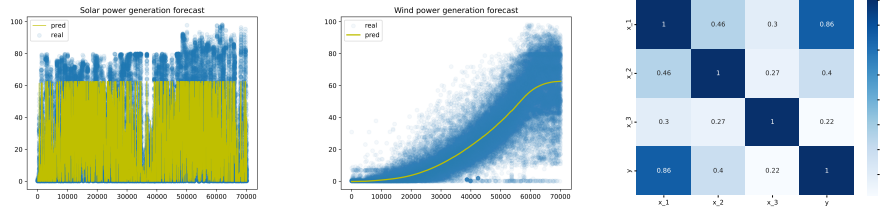
(a) Results of fitting the Airfoil-self-noise data (Eq.5) (b) Figure a after sorting by y_{pre} (c) Correlation coefficient matrix for Airfoil-self-noise



(d) Results of fitting the Airfoil-self-noise data (Eq.6) (e) Figure d after sorting by y_{pre} (f) Global temperature change prediction outcomes



(g) Solar energy power generation fitting result (h) Figure g after sorting by y_{pre}



(i) Wind energy power generation fitting result (j) Figure i after sorting by y_{pre} (k) The correlation matrix in wind energy prediction

Figure 2: Figure a and Figure b show the fitting results of Formula 5 for Scaled sound pressure level; Figure c displays the correlation coefficient matrix for various variables of Airfoil-self-noise; Figure d and Figure e show the fitting results of Formula 6 for Scaled sound pressure level. Figure f displays the fitting results of the Formula 7 for global temperature changes; Figure g and Figure h show the prediction results of Formula 8 for solar power generation; Figure i and Figure j display the fitting results of Formula 8 for wind power generation data; Figure k represents the correlation coefficient matrix of the variables used in the wind power generation data.

our algorithm only learned from four variables, x_1 , x_3 , x_4 , and x_5 , and missed variable x_2 . Although it may not seem like a perfect result, we can see from the correlation heatmap that variable x_2 has a high correlation with x_5 , with a correlation coefficient of 0.75, almost linearly related. Therefore, it is even wiser to retain x_5 and discard x_2 in the equation. This indirectly reflects the strong learning ability of our algorithm.

2.3.3 Modeling in environmental science (Prediction of Earth’s temperature change)[11].

Since the pre-industrial era, human emissions of carbon dioxide (CO₂), methane (CH₄), and nitrous oxide (N₂O) have made significant contributions to global warming. Therefore, exploring the relationship between greenhouse gas emissions and global average temperature changes has become an important goal of international climate research. Here, we applied the historical cumulative emissions of CO₂, CH₄, and N₂O between 1950 and 2022 to predict changes in the global average surface temperature. We used the data from the first 40 years as a training set and the data from the later 32 years as a testing set. The final results obtained from X-Net are as follows.

$$Y = 0.000450 * (x_1 + x_2 + x_3) - 7.61 * 10^{-8} \quad (7)$$

Here, Y represents the global average temperature change, x_1 represents the global cumulative CH₄ emissions in units of $(PgCO_2 - e_{100})$; x_2 represents the global cumulative CO₂ emissions in units of $(PgCO_2 - e_{100})$, and x_3 represents the global cumulative N₂O emissions in units of $(PgCO_2 - e_{100})$. The test results are shown in Figure 2f. Equation 7 clearly shows a direct proportionality between changes in global mean temperature and the sum of emissions from the three greenhouse gases.

2.3.4 Modeling in energy science (Solar And Wind Power Generation Forecasting)[12]

Accurate solar and wind power generation predictions are crucial for advanced electricity scheduling in energy systems. We used the solar and wind energy data provided by the State Grid Corporation of China to model the data. This data set consists of data directly collected from renewable energy stations, including generation and weather-related data from six wind farms and eight solar power stations distributed across different regions of China over the course of two years (2019-2020), collected every 15 minutes. The solar power generation data contains three main variables: Total solar irradiance(x_1), Air temperature(x_2), and Relative humidity(x_3). The solar energy generation prediction model obtained through training X-Net can be represented by equation 8, as follows:

$$Y = x_1(0.00044x_3(-0.00003x_1x_2 + 0.31) + 0.093) - 0.2466 \quad (8)$$

The fitted curves of the sun power are shown in Figure 2g and 2h. Note: Figure h underwent the same data sorting process as Figure b.

The wind power generation data also mainly includes three variables, Wind speed at

the height of the wheel hub(x_1), Wind direction at the height of the wheel hub(x_2), and Air temperature(x_3). The formula model obtained by X-Net for wind power generation using the above three variables as input can be represented by equation 9, as follows:

$$Y = x_1(0.0123x_1 + \frac{0.0123(x_1 - 1.53)}{0.00049x_1(x_1 - 15.93) + 0.049}) \quad (9)$$

The fitted curves of the wind power are shown in Figure 2i and 2j. Note: Figure j underwent the same data sorting process as Figure b. From Equation 9, we can see that X-Net has modeled the data well using only the first variable (wind speed) among the three variables. This is consistent with our understanding that wind power generation is mainly related to wind speed, which also aligns with reality. Furthermore, from the correlation coefficient heatmap 2k, we can clearly see that the correlation between x_1 (wind speed) and y (power generation) is as high as 0.86.

2.4 Ada- α function performance analysis

In the process of neural network training, whether the step size is appropriate directly affects the speed of network convergence. If the step size is excessively large, the optimal solution may be skipped, If the step size is too small, the convergence rate may be extremely sluggish, and the optimal solution may not be obtained within a predetermined number of iterations. Therefore, to improve network efficiency, we design a step-size dynamic adaptive function Ada- α . In order to test its performance, we selected four functions 'Nguyen-2', 'Nguyen-6', 'Nguyen-9', and 'Nguyen-10' from the Nguyen data set to test the Ada- α . Using the Ada- α function, we execute each of the formulas ten times, record the amount of time required to fully recover the formula, and then calculate an average. Then do the same for the case without the Ada- α function. The specific bar graph is depicted in Fig. ???. We can observe that when the Ada-*alpha* function is implemented, the network's convergence speed will increase dramatically.

3 Discussion

We propose a new neural network model X-Net, and the network structure of X-Net is not fixed but dynamically adapts to changes in real-time under the guidance of gradients. The structure and parameter redundancy of traditional artificial neural networks is greatly improved. Specifically, we design the network structure as a tree and in order to improve the representation ability of the neural network, we extend the activation function of the neural network to the activation function library, which not only contains the traditional activation functions such as [*ReLU, sigmoid*], but also includes the basic functions such as [$+$, $-$, \times , \div , *sin, cos, exp, sqrt, log*]. Next, we propose a new backpropagation mechanism, which can optimize not only the parameters of the network but also the activation function of the network nodes and the network structure. In particular, we take the output of each activation function as a variable E , differentiate the output of nodes of each layer through the chain rule, and then update it by the backpropagation algorithm. Finally, we select the activation function

of nodes according to the updated E .

X-Net outperforms state-of-the-art baselines in its ability to accurately fit the observed data. In particular, X-Net has better "extrapolation" than traditional regression algorithms. In addition, in order to further test X-Net's ability to aid scientific discovery, we tested X-Net's performance in multiple scientific fields, including social science, environmental science, energy science, and space science. In the end, X-Net came up with a good mathematical formula for modeling data in various disciplines and accurately reflected the relationship between the variables X and the predicted value Y in the data. For observational data in all of these areas, X-Net was able to summarize mathematical formulas that were concise, analyzable, and consistent with objective facts.

Moreover, inspired by people descending the mountain and combined with the problems existing in the gradient descent method, we proposed a step-size dynamic adaptive function Ada- α that can obviously improve the efficiency of convergence and can be widely applied to other deep learning domains.

Although the X-Net input in the article is two-dimensional and the output is one-dimensional, in fact, the dimensions of the input and output of X-Net are not explicitly limited. For example, if we remove the primary node from a tree of symbolic expressions, the output of the network becomes two-dimensional. So X-Net can also handle problems where the output is multi-dimensional. As a result, X-Net is theoretically capable of doing much of what ANN can do.

In future studies, We are going to explore the application area of X-Net in a near step. For example, we can develop a new recurrent neural network based on X-Net. We can also develop a new convolutional neural network by replacing the last fully connected layer of the convolutional neural network, etc.

4 Methods

Similar to the ANN, our algorithm consists mostly of two components: (1) Initialize a Tree-like network structure and perform forward propagation. (2) Utilize the Alternating backpropagation technique to update the parameters and activation function alternately. (3) Repeat the above process until the maximum number of iterations is reached, or the goodness of fit R^2 [13] reaches the set threshold and then stops the loop. The algorithm flow diagram for X-Net is shown in Fig. 3a. The detailed procedure of the algorithm is as follows: (i) The training data is obtained by sampling or observing. (ii) Obtain the data x, y_{noise} to be input into the network, then use the binary tree of the formula $x^2 + \sin(x)$ as the initialization structure of the network, and note the initialization constants W, B , where W is initialized to $[1, 1 \dots 1]$ and B is initialized to $[0, 0, \dots, 0]$. Then, using forward propagation, the predicted value y_{pre} is obtained, and MSE is calculated. (iii) Alternating Backpropagation, which involves taking partial derivatives with respect to constants and node outputs, If the condition $key\%ITE = 0$ is not satisfied, then the constants are updated. If the condition is met, the outputs of nodes with the value E are updated, followed by activation function updates via the Alternating Backpropagation mechanism. (iv) The previous procedure is repeated until a predetermined number of iterations or a predefined level

of accuracy is obtained. Fig. 3b depicts the macro comparison between our technique and the ANN. Fig. 3c describes the forward propagation process of our algorithm in detail. In the figure, E_i represents the output of the i^{th} node, w_i and b_i represent the two constants of the i^{th} node. The key distinction from ANN lies in the fact that we optimize not only the parameters W and b , but also treat the output E of each node as an optimizable variable, which undergoes alternate optimization with W and b . Subsequently, the activation function is updated based on the optimized E . A schematic of the dynamic adjustment of the network structure in the process of optimization is shown in Fig.3d. From the figure, we can see that the network structure and the neurons are adjusting in real time. We end up with the expression $y = \sin(x^2+x)+\sin(x)$.

4.1 Forward Propagation

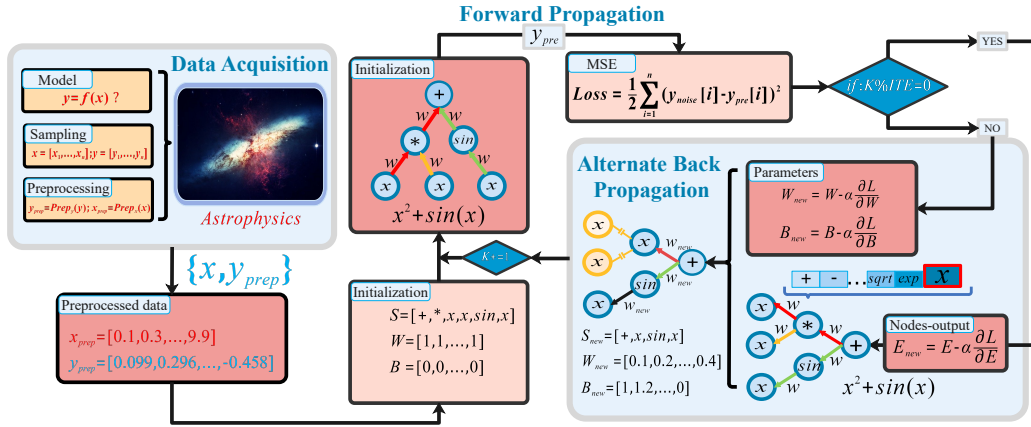
Firstly, we randomly initialize a tree-like neural network, and the activation function of neurons is assigned according to the rules so that the neural network can realize normal forward propagation. For example, if the activation function is $[relu, \sin]$ and so on, then the neuron only needs to have one input. But if the neuron is a binary activation function like $[+, -, \times, \div]$, then the input must be two. Since the network structure is a binary tree, we can expand the network in the order of preorder traversal. We assume that $S = [s_1, s_2, \dots, s_n]$ is of the neural network. And there is a one-to-one correspondence between network structures and the preorder traversal of neural networks. s_i in S indicates that the neural network preorder traverses the i^{th} Activation functions of neurons including unary activation functions $[ReLU, sigmoid, \sin, \cos, \log, exp, sqrt, \dots]$, Binary activation function $[+, -, \times, \div]$, and the leaf node symbols (x_1, x_2, \dots, x_n) . We start by randomly initializing a tree neural network, which in particular can be represented by a mathematical expression $x^2 + \sin(x)$. The network structure is shown in Fig. ???. For each node in the neural network, whether it is a leaf node or an intermediate node, we will have two constants, such as the node $\sin(x)$ in the above network, for this node we have two parameters d_1 and b_1 , namely its output is $d_1 \sin(x) + b_1$. After forward propagation, the final output of the neural network is \hat{y} . And then we define the loss function as the mean square error (MSE)[14] whose formula is as follows(10):

$$Loss = \frac{1}{N} \sum_{i=0}^N (y_i - \hat{y}_i)^2 \quad (10)$$

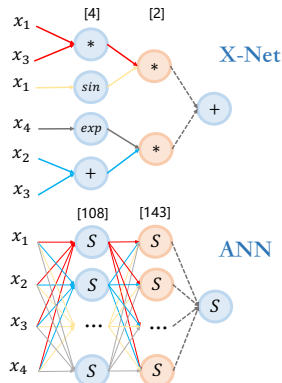
Where N is the number of sampling points, y_i is the true label value of the i_{th} sample, and \hat{y}_i is the predicted value of the i^{th} sample. The objective is to continuously update the node symbols and parameters using the back-propagation technique so that the loss function value decreases over time.

4.2 Alternating Backpropagation

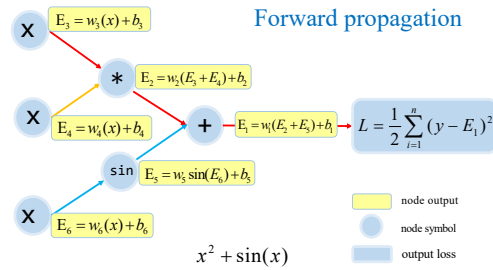
Similar to the backpropagation of the ANN, Alternating Backpropagation also use the chain rule to calculate the gradient of each layer of the X-Net. It's just that



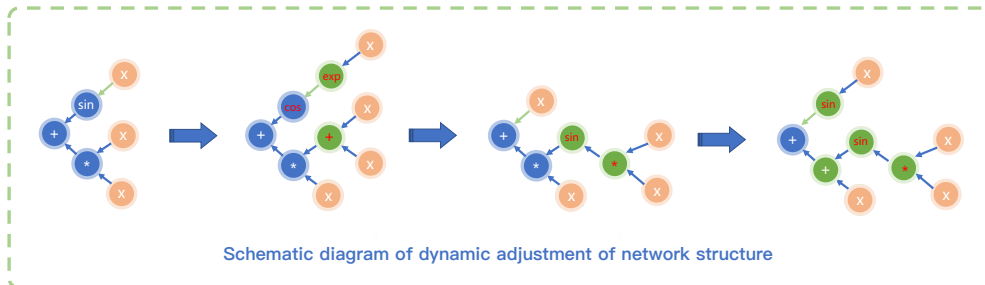
(a) The overall flowchart of X-Net



(b) Comparison between X-Net and ANN structures



(c) Schematic of X-Net forward propagation



(d) Schematic diagram of structural changes during the training process

Figure 3: Figure a illustrates the algorithmic flowchart of X-Net; From Figure b, we observe a performance discrepancy between X-Net and ANN in the same regression task, with X-Net having a significantly lower network complexity compared to ANN; The Figure c describes the forward propagation process of our algorithm in detail; Figure d illustrates the dynamic changes in the network structure of X-Net during the training process.

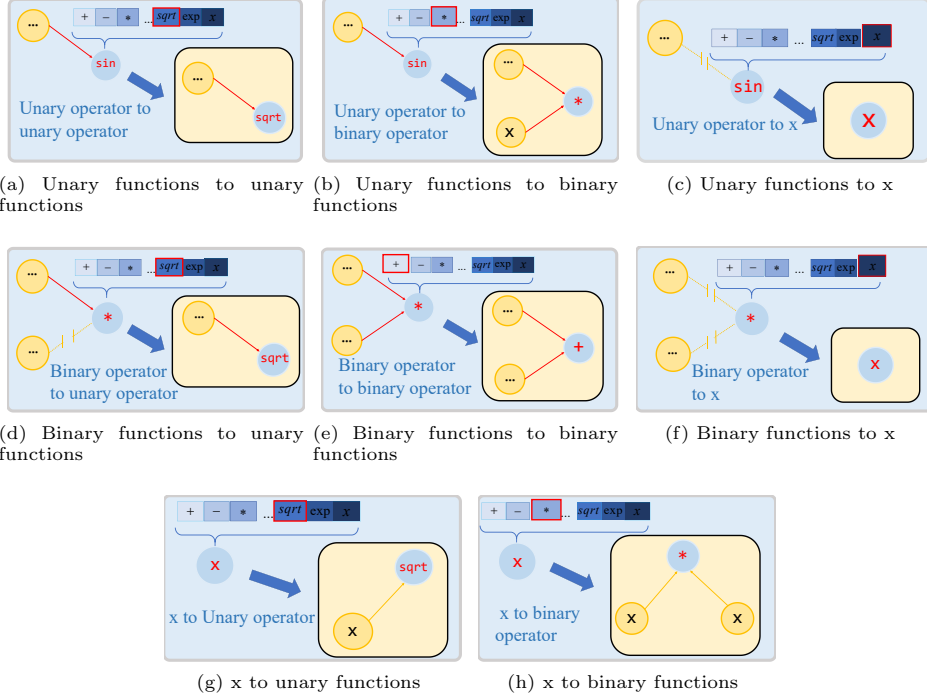


Figure 4: This illustration depicts the evolutionary process among different neurons. This mechanism ensures that the neural network can still conduct forward propagation normally during its growth and evolution. The operator circled in red is the selected operator. Herein, the neuron types selected after differential gene expression are delineated by red boxes.

Alternating Backpropagation alternately update the activation function and parameters of the neural network during backpropagation. In the process of Alternating Backpropagation, we treat the output of each neurons as a optimizabale variable \mathcal{E} , $\mathcal{E} = f(\mathcal{E}_{left}, \mathcal{E}_{right})$, where \mathcal{E} is the output of the current node, \mathcal{E}_{left} is the output of the left node of the current node, \mathcal{E}_{right} is the output of the right node of the current node, f is The numerical computation corresponding to the node activate function. First, take the partial derivative of \mathcal{E} with respect to the loss function, and then calculate the partial derivative of the \mathcal{E}_{left} and \mathcal{E}_{right} with respect to the loss function by the chain rule[15]. Finally, update them with the stochastic gradient descent(SGD)[16, 17] (It can also be other numerical optimization algorithms, such as BFGS and so on). Similar to a conventional ANN, we utilize SGD to update the network's constants, $w_{new} = w - \alpha * \frac{\partial Loss}{\partial w}$, Where w_{new} is the updated constant, w is the constant without updating, α is the learning rate, $\frac{\partial Loss}{\partial w}$ is the partial derivative of the loss function to w . For example, for the neural network architecture shown in Fig. 3c, Through the Alternating Backpropagation, we obtain the gradient of each node's output \mathcal{E}_n and its corresponding two constants w_n, b_n . Then, we optimize activate

function and parameters in alternation. The specific formula is deduced as follows:

$$d\mathcal{E}_1 = \frac{\partial \mathcal{L}}{\partial \mathcal{E}_1} \quad (11)$$

$$dw_1 = \frac{\partial \mathcal{L}}{\partial \mathcal{E}_1} \frac{\partial E_1}{\partial w_1} = d\mathcal{E}_1 \frac{\partial E_1}{\partial w_1} \quad (12)$$

$$db_1 = \frac{\partial \mathcal{L}}{\partial \mathcal{E}_1} \frac{\partial \mathcal{E}_1}{\partial b_1} = d\mathcal{E}_1 \frac{\partial \mathcal{E}_1}{\partial b_1} = d\mathcal{E}_1 \quad (13)$$

$$d\mathcal{E}_2 = \frac{\partial \mathcal{L}}{\partial \mathcal{E}_2} = \frac{\partial \mathcal{L}}{\partial \mathcal{E}_1} \frac{\partial \mathcal{E}_1}{\partial \mathcal{E}_2} = d\mathcal{E}_1 \frac{\partial \mathcal{E}_1}{\partial \mathcal{E}_2} \quad (14)$$

$$dw_2 = \frac{\partial \mathcal{L}}{\partial w_2} = \frac{\partial \mathcal{L}}{\partial \mathcal{E}_1} \frac{\partial \mathcal{E}_1}{\partial \mathcal{E}_2} \frac{\partial \mathcal{E}_2}{\partial w_2} = d\mathcal{E}_2 \frac{\partial \mathcal{E}_2}{\partial w_2} \quad (15)$$

$$db_2 = \frac{\partial \mathcal{L}}{\partial b_2} = \frac{\partial \mathcal{L}}{\partial \mathcal{E}_1} \frac{\partial \mathcal{E}_1}{\partial \mathcal{E}_2} \frac{\partial \mathcal{E}_2}{\partial b_2} = d\mathcal{E}_2 \frac{\partial \mathcal{E}_2}{\partial b_2} = d\mathcal{E}_2 \quad (16)$$

$$d\mathcal{E}_3 = \frac{\partial \mathcal{L}}{\partial \mathcal{E}_3} = \frac{\partial \mathcal{L}}{\partial \mathcal{E}_1} \frac{\partial \mathcal{E}_1}{\partial \mathcal{E}_2} \frac{\partial \mathcal{E}_2}{\partial \mathcal{E}_3} = d\mathcal{E}_2 \frac{\partial \mathcal{E}_2}{\partial \mathcal{E}_3} \quad (17)$$

$$dw_3 = \frac{\partial \mathcal{L}}{\partial w_3} = \frac{\partial \mathcal{L}}{\partial \mathcal{E}_1} \frac{\partial \mathcal{E}_1}{\partial \mathcal{E}_2} \frac{\partial \mathcal{E}_2}{\partial \mathcal{E}_3} \frac{\partial \mathcal{E}_3}{\partial w_3} = d\mathcal{E}_3 \frac{\partial \mathcal{E}_3}{\partial w_3} \quad (18)$$

$$db_3 = \frac{\partial \mathcal{L}}{\partial b_3} = \frac{\partial \mathcal{L}}{\partial \mathcal{E}_1} \frac{\partial \mathcal{E}_1}{\partial \mathcal{E}_2} \frac{\partial \mathcal{E}_2}{\partial \mathcal{E}_3} \frac{\partial \mathcal{E}_3}{\partial b_3} = d\mathcal{E}_3 \frac{\partial \mathcal{E}_3}{\partial b_3} = d\mathcal{E}_3 \quad (19)$$

...

Update the parameters:

$$w_{1-new} = w_1 - \alpha dw_1 \quad (20)$$

$$w_{2-new} = w_2 - \alpha dw_2 \quad (21)$$

$$w_{3-new} = w_3 - \alpha dw_3 \quad (22)$$

$$b_{1-new} = b_1 - \alpha db_1 \quad (23)$$

$$b_{2-new} = b_2 - \alpha db_2 \quad (24)$$

$$b_{3-new} = b_3 - \alpha db_3 \quad (25)$$

...

$$\mathcal{E}_{1-new} = \mathcal{E}_1 - \alpha d\mathcal{E}_1 \quad (26)$$

$$\mathcal{E}_{2-new} = \mathcal{E}_2 - \alpha d\mathcal{E}_2 \quad (27)$$

$$\mathcal{E}_{3-new} = \mathcal{E}_3 - \alpha d\mathcal{E}_3 \quad (28)$$

...

4.3 Selection of Neuronal Types (differential gene expression.)

After backpropagation, we update the output \mathcal{E} of each neuron in the direction of gradient descent. $\mathcal{E}_{i-new} = \mathcal{E}_i - \alpha \frac{\partial L}{\partial \mathcal{E}_i}$, The updated neuron output is arranged according to the preorder traversal as $\mathcal{E}_{new} = [\mathcal{E}_{1-new}, \mathcal{E}_{2-new}, \dots, \mathcal{E}_{n-new}]$, For the updated output value of each neuron, we update the activate function in turn according to the following method. For the i^{th} node, Suppose its symbol is $+$, that is, $\mathcal{E}_{i-old} = \mathcal{E}_{l-old} + \mathcal{E}_{r-old}$, where \mathcal{E}_{l-old} is the output of the left node of the i^{th} node, \mathcal{E}_{r-old} is the output of the right node of the i^{th} node. Assuming that the output value of the i^{th} node is updated to \mathcal{E}_{i-new} , and its left and right child nodes are updated to be \mathcal{E}_{l-new} and \mathcal{E}_{r-new} , respectively. We denote them as $\mathcal{E}_{left}, \mathcal{E}_{right}$, Then these two values are taken as inputs into the activation function library. (the unary activate function uses only the \mathcal{E}_{left} as input), and get the output list: $[\mathcal{E}_{left} + \mathcal{E}_{right}, \mathcal{E}_{left} - \mathcal{E}_{right}, \mathcal{E}_{left} * \mathcal{E}_{right}, \mathcal{E}_{left} \div \mathcal{E}_{right}, \sin(\mathcal{E}_{left}), \cos(\mathcal{E}_{left}), \log(\mathcal{E}_{left}), \sqrt{\mathcal{E}_{left}}, e^{\mathcal{E}_{left}}, \text{relu}(x), \text{sigmoid}(x), x]$. These output values correspond to the 12 activation functions of $[+, -, \times, \div, \sin, \cos, \log, \text{sqrt}, \text{exp}, \text{relu}, \text{sigmoid}, x]$. Then we make the difference between these 12 outputs and \mathcal{E}_{i-new} respectively and then take the absolute value to get $G = [g_1, g_2, \dots, g_{12}]$. Next, we choose the smallest of the G , and then, if this value is also less than the preset threshold(e.g.0.01), we use its corresponding activate function as the new activate function for the i^{th} node. Other nodes are analogous.

4.4 Substitution of Activation Functions (Neuronal Evolution)

In order to ensure that the network can still forward propagation normally after the structure and neuron activation function are updated. For instance, the x node can no longer contain child nodes, the binary activate function requires two child nodes, etc. For this purpose we have established the following rules:(1) When the unary activate function becomes a unary activate function, the node symbol is directly transformed, and the others do not make any changes. (2) When the unary activate function is transformed into a binary activate function, the original child node of the unary activate function is retained, and the other child node of None is replaced by x. (3) When the binary activate function becomes a binary activate function, the node symbol is directly changed, and no other changes are made. (4), when the binary activate function is transformed into the unary activate function, there are two situations at this time. a, when it is better to use the output of the left child node as the input, only keep the left child node. When the output of the right child node is used as the input and the result is better, only the right child node is kept. (3), regardless of any activate function, if it becomes x, all nodes whose main node is this node will become None. (4), there are two cases when x becomes an activate function. a, if x becomes a unary activate function, the node symbol becomes a unary activate function, and the left node is added to the leaf node x. When x becomes a binary operator, the node becomes a binary activate function, and the left and right nodes are added, both of which are leaf nodes x. The specific operator replacement process is shown more vividly in Fig. 4.

4.5 Restrictions and handling of numerical computing

To avoid infinite values "inf" and NaN values during forward and backward propagation, we place some restrictions on computation, (1) To prevent numerical overflow, the output values of all nodes are truncated during the computation process[18], Assuming that the output value of a node is \mathcal{E} , we allow the maximum output range to be $[-V, +V]$, then, when $|\mathcal{E}| \geq V$, $\mathcal{E} = \frac{\mathcal{E}}{|\mathcal{E}|} * V$ (2) In order to prevent the gradient from disappearing or exploding during the backpropagation of the network, we truncate the gradient and limit the gradient range[19, 20]. Assuming that the value of the gradient is g , the output range is $[-G_{max}, -G_{min}] \cup [G_{min}, G_{max}]$, When $|g| \geq G_{max}$ or $|g| \leq G_{min}$, The values of g are respectively: $g = \frac{g}{|g|} * G_{max}$ and $g = \frac{g}{|g|} * G_{min}$. (3) We restrict the generation of some unreasonable operations. such as for $\log(x)$, where the value of x must be greater than 0, Therefore, operators with negative values in the range cannot be in the position of x . For example, $\log(\sin(x))$, $\sqrt{\cos(x)}$ and similar operations are not allowed.

4.6 Avoid getting stuck in local optimum

In the process of optimization and training, the network is likely to fall into a local optimum if no additional conditions are added[21]. In order to prevent this from happening as much as possible, we set a count value of *count*. Whenever the network loss does not change or increase, the *count* increases by 1. When the *count* reaches a certain threshold, we arbitrarily select a node of the neural network, and arbitrarily change its activate function to other functions in the activate function library, By adding such a "disturbance", the algorithm can jump out of the local optimum as much as possible. We found through experiments that better results can be obtained when the threshold value is 20.

4.7 Step size adaptation function: Ada- α

In the process of network training, the step size has an extremely important influence on the convergence speed of the network and whether the optimal solution can be found[22–24]. Therefore, in order to better adapt to the algorithm and make the algorithm achieve better results, we designed an Ada- α that can adaptively and dynamically adjust the step size according to the network training situation. The formula for Ada- α is as follows(29):

$$\alpha = \frac{\tanh(e^{-|Loss[-2]-Loss[-1]|})}{a}. \quad (29)$$

$Loss[-2]$ represents the loss value of the previous iteration, $Loss[-1]$ represents the loss value of the current iteration, and a is the hyperparameter for adjusting the step size range. The Ada- α is inspired by people going down the mountain. For example, when we are descending a relatively steep hill, our bodies will lean back, one small step at a time. And when the mountain is relatively flat, we will boldly take big strides forward. As we were walking, the altitude we were at suddenly increased. This may be because our stride is too big, "fly" to the other side of the mountain. At this moment, we should take smaller steps to prevent us from striding in the wrong

direction. Inspired by this, we propose the Ada- α . When the value of the front and rear loss functions decreases greatly, we make the step size α smaller. When the value of the front and rear loss functions decreases relatively small, we make the step size α larger. When the value of the front and rear loss functions rises. That means step size α is too big, and we're flying to the other side of the mountain, so we're going to make α smaller.

5 Acknowledgments

This work was supported in part by the National Natural Science Foundation of China under Grant 92370117, in part by CAS Project for Young Scientists in Basic Research under Grant YSBR-090, and in part by the Key Research Program of the Chinese Academy of Sciences under Grant XDPB22

References

- [1] Thomas Bäck and Hans-Paul Schwefel. An overview of evolutionary algorithms for parameter optimization. *Evolutionary computation*, 1(1):1–23, 1993.
- [2] Peter I Frazier. A tutorial on bayesian optimization. *arXiv preprint arXiv:1807.02811*, 2018.
- [3] Barret Zoph and Quoc V Le. Neural architecture search with reinforcement learning. *arXiv preprint arXiv:1611.01578*, 2016.
- [4] Esteban Real, Sherry Moore, Andrew Selle, Saurabh Saxena, Yutaka Leon Sue-matsu, Jie Tan, Quoc V Le, and Alexey Kurakin. Large-scale evolution of image classifiers. In *International conference on machine learning*, pages 2902–2911. PMLR, 2017.
- [5] Masanori Suganuma, Shinichi Shirakawa, and Tomoharu Nagao. A genetic programming approach to designing convolutional neural network architectures. In *Proceedings of the genetic and evolutionary computation conference*, pages 497–504, 2017.
- [6] Shinichi Shirakawa, Yasushi Iwata, and Youhei Akimoto. Dynamic optimization of neural network structures using probabilistic modeling. In *Proceedings of the AAAI Conference on Artificial Intelligence*, volume 32, 2018.
- [7] Ameya D Jagtap, Yeonjong Shin, Kenji Kawaguchi, and George Em Karniadakis. Deep kronecker neural networks: A general framework for neural networks with adaptive activation functions. *Neurocomputing*, 468:165–180, 2022.
- [8] Forest Agostinelli, Matthew Hoffman, Peter Sadowski, and Pierre Baldi. Learning activation functions to improve deep neural networks. *arXiv preprint arXiv:1412.6830*, 2014.

- [9] Deng-Kui Li, Chang-Lin Mei, and Ning Wang. Tests for spatial dependence and heterogeneity in spatially autoregressive varying coefficient models with application to boston house price analysis. *Regional Science and Urban Economics*, 79: 103470, 2019.
- [10] Thomas Brooks, D. Pope, and Michael Marcolini. Airfoil Self-Noise. UCI Machine Learning Repository, 2014. DOI: <https://doi.org/10.24432/C5VW2C>.
- [11] Matthew W Jones, Glen P Peters, Thomas Gasser, Robbie M Andrew, Clemens Schwingshackl, Johannes Gütschow, Richard A Houghton, Pierre Friedlingstein, Julia Pongratz, and Corinne Le Quéré. National contributions to climate change due to historical emissions of carbon dioxide, methane, and nitrous oxide since 1850. *Scientific Data*, 10(1):155, 2023.
- [12] Yongbao Chen and Junjie Xu. Solar and wind power data from the chinese state grid renewable energy generation forecasting competition. *Scientific Data*, 9(1): 577, 2022.
- [13] Theodore W Anderson and Donald A Darling. A test of goodness of fit. *Journal of the American statistical association*, 49(268):765–769, 1954.
- [14] Cort J Willmott and Kenji Matsuura. Advantages of the mean absolute error (mae) over the root mean square error (rmse) in assessing average model performance. *Climate research*, 30(1):79–82, 2005.
- [15] Vasily E Tarasov. On chain rule for fractional derivatives. *Communications in Nonlinear Science and Numerical Simulation*, 30(1-3):1–4, 2016.
- [16] Léon Bottou. Stochastic gradient descent tricks. In *Neural networks: Tricks of the trade*, pages 421–436. Springer, 2012.
- [17] Gergely Neu, Gintare Karolina Dziugaite, Mahdi Haghifam, and Daniel M Roy. Information-theoretic generalization bounds for stochastic gradient descent. In *Conference on Learning Theory*, pages 3526–3545. PMLR, 2021.
- [18] Karim Abbas. Multiplications to multipliers: Performing arithmetic in hardware. In *From Algorithms to Hardware Architectures*, pages 49–85. Springer, 2023.
- [19] Christopher Aicher, Nicholas J Foti, and Emily B Fox. Adaptively truncating backpropagation through time to control gradient bias. In *Uncertainty in Artificial Intelligence*, pages 799–808. PMLR, 2020.
- [20] Sekitoshi Kanai, Yasuhiro Fujiwara, and Sotetsu Iwamura. Preventing gradient explosions in gated recurrent units. *Advances in neural information processing systems*, 30, 2017.

- [21] Wu Deng, Junjie Xu, and Huimin Zhao. An improved ant colony optimization algorithm based on hybrid strategies for scheduling problem. *IEEE access*, 7: 20281–20292, 2019.
- [22] Christian Daniel, Jonathan Taylor, and Sebastian Nowozin. Learning step size controllers for robust neural network training. In *Thirtieth AAAI Conference on Artificial Intelligence*, 2016.
- [23] Steven K Esser, Jeffrey L McKinstry, Deepika Bablani, Rathinakumar Appuswamy, and Dharmendra S Modha. Learned step size quantization. *arXiv preprint arXiv:1902.08153*, 2019.
- [24] Liyuan Liu, Haoming Jiang, Pengcheng He, Weizhu Chen, Xiaodong Liu, Jianfeng Gao, and Jiawei Han. On the variance of the adaptive learning rate and beyond. *arXiv preprint arXiv:1908.03265*, 2019.

Appendix A Section title of first appendix

Algorithm 1 Pseudocode for X-Net.

```
1: Initialize:  $\mathcal{S} = [s_1, s_2, \dots, s_m]$ ;  $\mathcal{D} = [d_1, d_2, \dots, d_m]$ ;  $\mathcal{B} = [b_1, b_2, \dots, b_m]$ ;  $\mathcal{X} = [x_1, x_2, \dots, x_n]$ ;  $\mathcal{Y} = [y_1, y_2, \dots, y_n]$ 
2: for  $j = 0$  to  $ite$  do
3:    $\mathcal{S} \leftarrow \mathcal{S}_{best}$ 
4:    $\mathcal{D} \leftarrow \mathcal{D}_{best}$ 
5:    $\mathcal{B} \leftarrow \mathcal{B}_{best}$ 
6:   for  $i = 0$  to  $n$  do
7:     for  $k = 0$  to  $100$  do
8:       The nodes:  $\mathcal{A} = [a_1, a_2, \dots, a_m]$ 
9:       Constructing a neural network:  $\mathcal{A} \leftarrow \mathcal{S}$ 
10:      for  $k = 0$  to  $m$  do
11:         $\mathcal{A}[k] \leftarrow \mathcal{S}[k]$ 
12:      end for
13:       $\mathcal{E} = [\mathcal{E}_1, \mathcal{E}_2, \dots, \mathcal{E}_m]$ 
14:      for  $k = 0$  to  $m$  do
15:         $\mathcal{E}[k] \leftarrow d_k * s_k(x_i) + b_k$ 
16:      end for
17:       $\hat{y} \leftarrow \mathcal{E}[0]$ 
18:       $loss \leftarrow \frac{1}{2}(y_i - \hat{y})^2$ 
19:       $\mathcal{E}_{all} = f(X)$ 
20:       $\mathcal{R}^2 = r2(\mathcal{E}_{all}, y)$ 
21:      SaveBest( $\mathcal{S}, \mathcal{R}^2$ )
22:      Train( $key, \mathcal{E}, \mathcal{D}, \mathcal{B}$ )
23:    end for
24:  end for
25: end for
```

Appendix B

Algorithm 2 SaveBest

```
1: Variables:  $R^2$ ;  $R_{best}$ 
2: Start:
3: if  $R^2 \geq R_{best}$  then
4:    $\mathcal{R}_{best} \leftarrow R^2$ 
5:    $\mathcal{S}_{best} \leftarrow \mathcal{S}$ 
6:    $\mathcal{D}_{best} \leftarrow \mathcal{D}$ 
7:    $\mathcal{B}_{best} \leftarrow \mathcal{B}$ 
8: end if
```

Appendix C

Algorithm 3 Train

Variables: key ; $\mathcal{E} = [\mathcal{E}_1, \mathcal{E}_2, \dots, \mathcal{E}_m]$;
 $\mathcal{D} = [d_1, d_2, \dots, d_m]$, $\mathcal{B} = [b_1, b_2, \dots, b_m]$
if $key \bmod ITE \neq 0$ **then**
 $\mathcal{D}_{new}[k] \leftarrow \mathcal{D}[k] - \alpha \frac{\partial L}{\partial \mathcal{D}[k]}$
 $\mathcal{B}_{new}[k] \leftarrow \mathcal{B}[k] - \alpha \frac{\partial L}{\partial \mathcal{B}[k]}$
end if
if $key \bmod ITE = 0$ **then**
 for $k = 0$ to m **do**
 $\mathcal{E}_{new}[k] \leftarrow \mathcal{E}[k] - \alpha \frac{\partial L}{\partial \mathcal{E}[k]}$
 end for
 UpdateSymbols(\mathcal{E})
end if

Appendix D

Algorithm 4 UpdateSymbols

1: Variables: key ; $\mathcal{E}_{new} = [\mathcal{E}_{1new}, \mathcal{E}_{2new}, \dots, \mathcal{E}_{mnew}]$;
2: *activation functions* = $[+, -, *, /, \sin, \cos, \text{sqrt}, \log, \text{exp}, \text{sigmoid}, \text{relu}, x]$
3: **for** $k = 0$ to m **do**
4: $\mathcal{SY} \leftarrow \{\mathcal{E}[k]_{newl} + \mathcal{E}[k]_{newr}, \mathcal{E}[k]_{newl} - \mathcal{E}[k]_{newr},$
5: $\mathcal{E}[k]_{newl} * \mathcal{E}[k]_{newr}, \mathcal{E}[k]_{newl} / \mathcal{E}[k]_{newr},$
6: $\sin(\mathcal{E}[k]_{newl}), \cos(\mathcal{E}[k]_{newl}), \text{sqrt}(\mathcal{E}[k]_{newl}),$
7: $\log(\mathcal{E}[k]_{newl}), \text{exp}(\mathcal{E}[k]_{newl}), \text{sigmoid}(\mathcal{E}[k]_{newl}),$
8: $\text{relu}(\mathcal{E}[k]_{newl}), x\}$
9: $Choice \leftarrow |\mathcal{SY} - \mathcal{E}[k]_{new}|$
10: $Index \leftarrow \arg \min(Choice)$
11: $S[k] \leftarrow \text{activation functions}[Index]$
12: **end for**

Appendix E

Table E1

SYMBOL LIBRARY AND VALUE RANGE OF THE THREE DATA SETS NGUYEN, KORNS,
AND JIN.

Name	Expression
Nguyen-1	$x_1^3 + x_1^2 + x_1$
Nguyen-2	$x_1^4 + x_1^3 + x_1^2 + x_1$
Nguyen-3	$x_1^5 + x_1^4 + x_1^3 + x_1^2 + x_1$
Nguyen-4	$x_1^6 + x_1^5 + x_1^4 + x_1^3 + x_1^2 + x_1$
Nguyen-5	$\sin(x_1^2) \cos(x) - 1$
Nguyen-6	$\sin(x_1) + \sin(x_1 + x_1^2)$
Nguyen-7	$\log(x_1 + 1) + \log(x_1^2 + 1)$
Nguyen-8	\sqrt{x}
Nguyen-9	$\sin(x) + \sin(x_2^2)$
Nguyen-10	$2 \sin(x) \cos(x_2)$
Nguyen-11	$x_1^{x_2}$
Nguyen-12	$x_1^4 - x_1^3 + \frac{1}{2}x_2^2 - x_2$

Appendix F

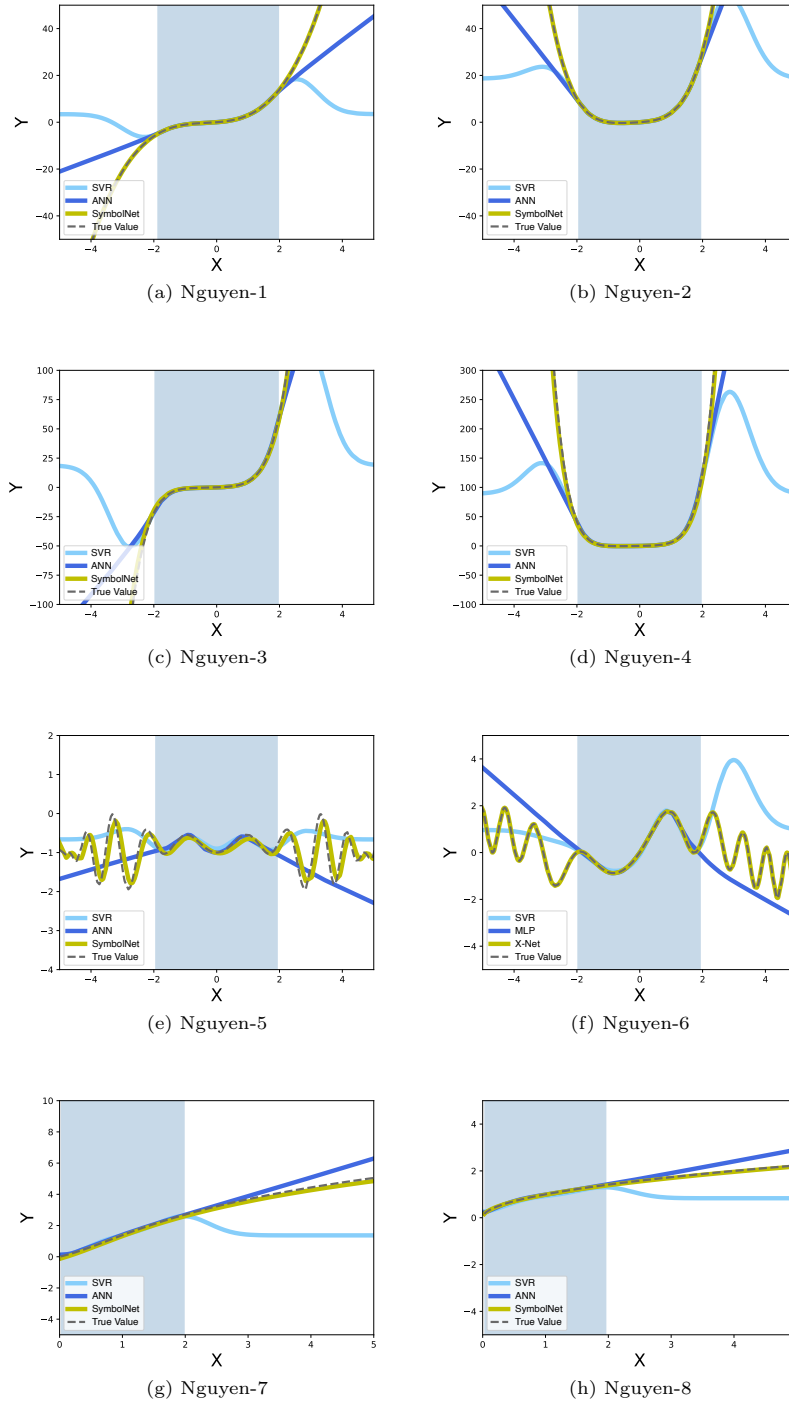


Figure F1: This figure shows the extrapolation of the three algorithms on the unary formula in the Nguyen data set in Table 1.

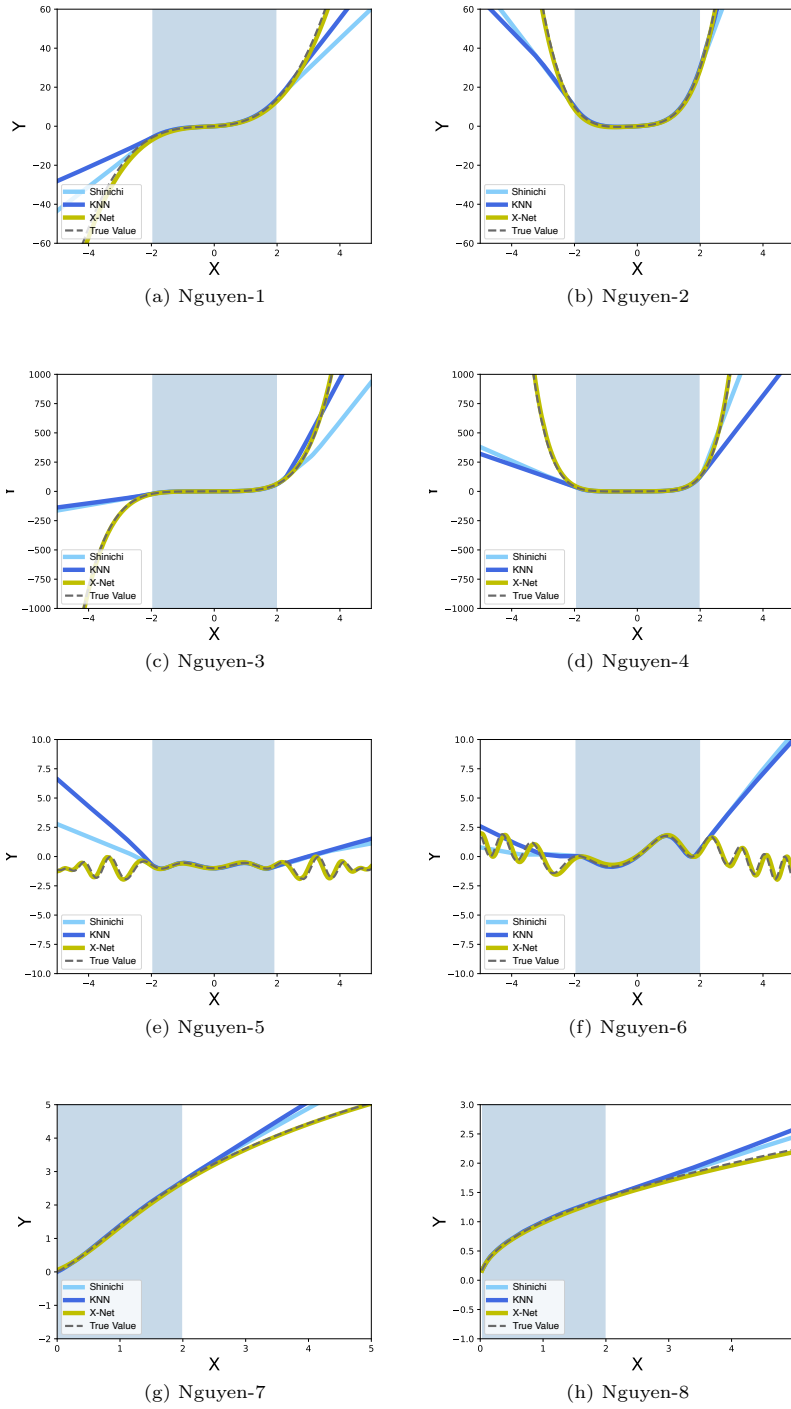
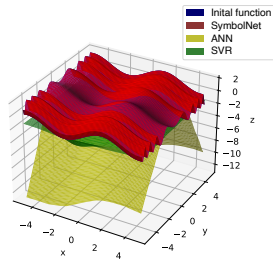
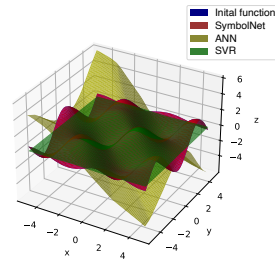


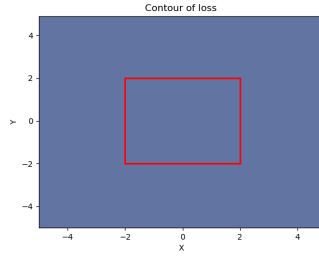
Figure F2: This figure shows the extrapolation of the three algorithms on the unary formula in the Nguyen data set in Table 1.



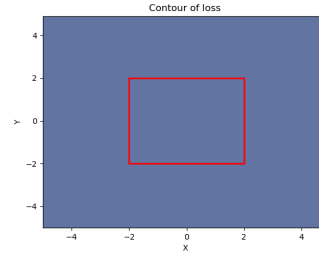
(a) Nguyen-9



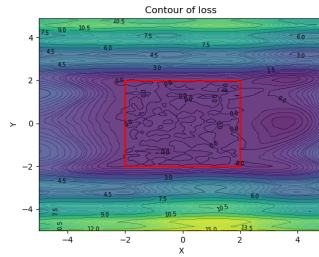
(b) Nguyen-10



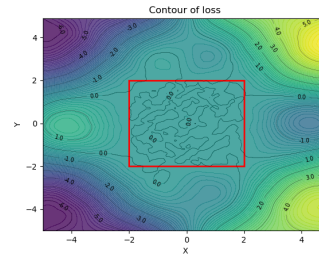
(c) Nguyen-9-X-Net



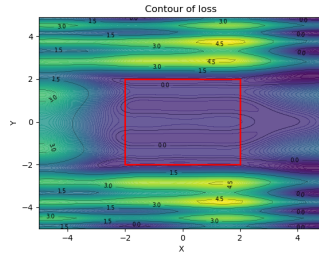
(d) Nguyen-10-X-Net



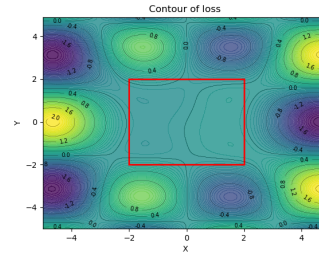
(e) Nguyen-9-ANN



(f) Nguyen-10-ANN

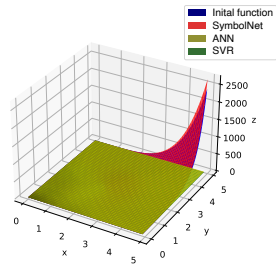


(g) Nguyen-9-SVR

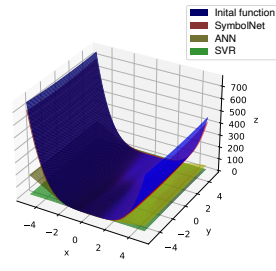


(h) Nguyen-10-SVR

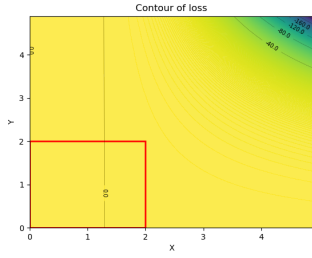
Figure F3: This figure shows the test results of our algorithm, ANN, and SVR on the Nguyen-9 and Nguyen-10 in Table 1. To see the difference between the predicted surface and the real surface in the range $[-2,2]$ and outside the range, we drew the contour plots after the difference between the predicted surface and the real surface of the three algorithms respectively.



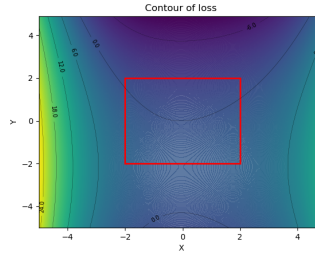
(a) Nguyen-11



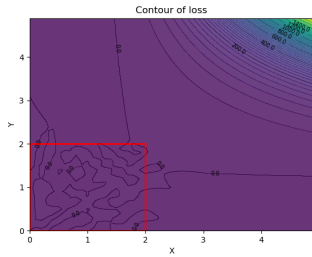
(b) Nguyen-12



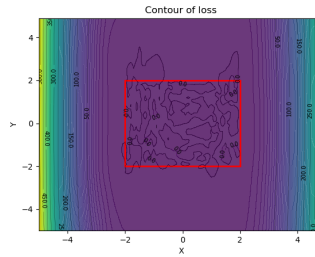
(c) Nguyen-11-X-Net



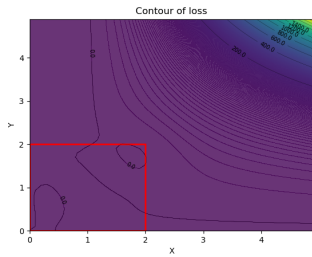
(d) Nguyen-12-X-Net



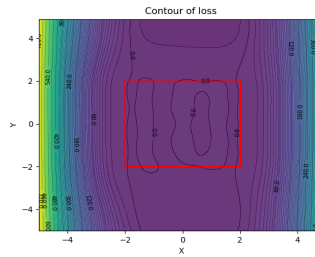
(e) Nguyen-11-ANN



(f) Nguyen-12-ANN

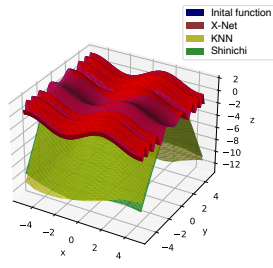


(g) Nguyen-11-SVR

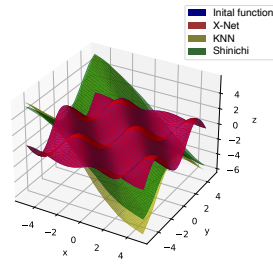


(h) Nguyen-12-SVR

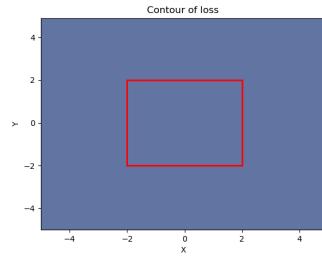
Figure F4: This figure shows the test results of our algorithm, ANN, and SVR on the Nguyen-11 and Nguyen-12 in Table 1. To clearly see the difference between the predicted surface and the real surface in the range $[-2,2]$ and outside the range, We calculate the difference between the prediction planes of the three algorithms and the actual plane respectively, then plot the contour lines.



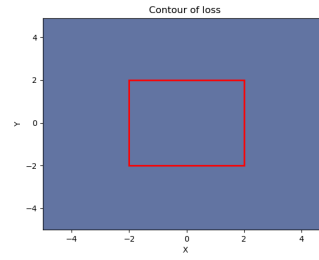
(a) Nguyen-9



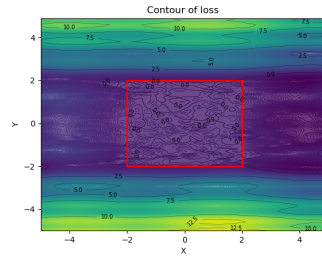
(b) Nguyen-10



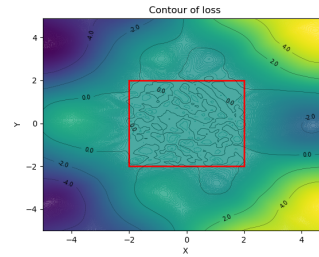
(c) Nguyen-9-X-Net



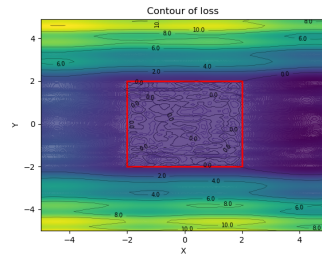
(d) Nguyen-10-X-Net



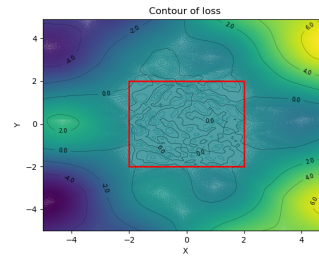
(e) Nguyen-9-Kronecker NN



(f) Nguyen-10-Kronecker NN

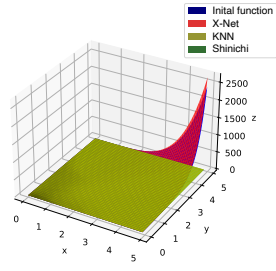


(g) Nguyen-9-Shinichi

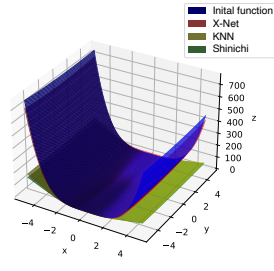


(h) Nguyen-10-Shinichi

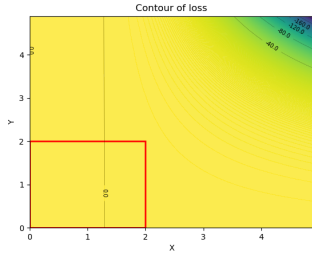
Figure F5: This figure shows the test results of our algorithm, Kronecker NN, and Shinichi on the Nguyen-9 and Nguyen-10 in Table 1. In order to clearly see the difference between the predicted surface and the real surface in the range $[-2, 2]$ and outside the range, We calculate the difference between the prediction planes of the three algorithms and the actual plane respectively, then plot the contour lines.



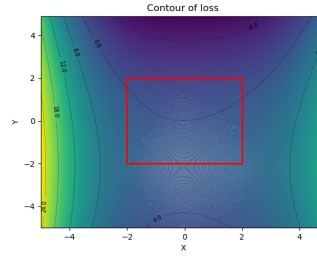
(a) Nguyen-11



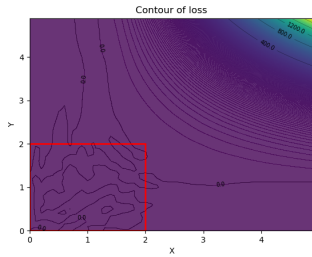
(b) Nguyen-12



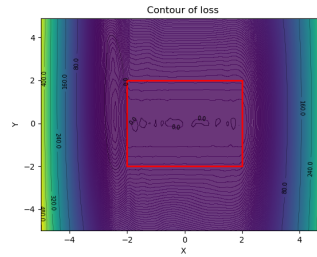
(c) Nguyen-11-X-Net



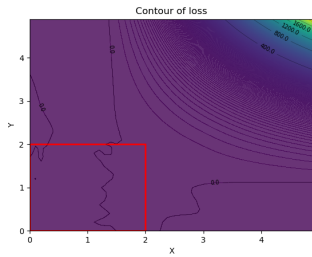
(d) Nguyen-12-X-Net



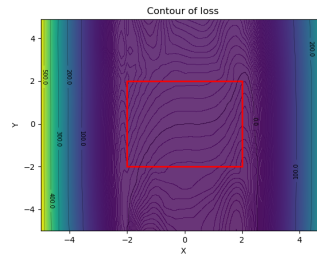
(e) Nguyen-11-Kronecker NN



(f) Nguyen-12-Kronecker NN



(g) Nguyen-11-Shinichi



(h) Nguyen-12-Shinichi

Figure F6: This figure shows the test results of our algorithm, Kronecker NN, and Shinichi on the Nguyen-11 and Nguyen-12 in Table 1. In order to clearly see the difference between the predicted surface and the real surface in the range $[-2, 2]$ and outside the range, We calculate the difference between the prediction planes of the three algorithms and the actual plane respectively, then plot the contour lines.